# FINAL TECHNICAL REPORT

| | |
|---|---|
| **Federal Agency:** | DOE/EERE/Advanced Materials and Manufacturing Technologies Office (AMMTO) |
| **Award Number:** | DE-EE0009105 |
| **Project Title:** | Novel ceramic capacitors with ultrahigh energy density and efficiency |
| **Project Period:** | 7/1/2020 – 6/30/2024 |
| **Recipient Organization:** | Iowa State University<br>New York University (Subrecipient) |
| **Principal Investigator:** | **Professor Xiaoli Tan**<br>Department of Materials Science and Engineering<br>Iowa State University<br>Email: xtan@iastate.edu<br>Phone: 515-294-3355 |
| **Team Member:** | **Professor Jun Cui**<br>Department of Materials Science and Engineering<br>Iowa State University<br><br>**Professor Duane D. Johnson**<br>Department of Materials Science and Engineering<br>Iowa State University<br><br>**Professor Chinmay Hegde**<br>Tandon School of Engineering<br>New York University |

## Executive Summary

Antiferroelectric ceramics are a special class of material that have shown great potential as the dielectric in electrical capacitors due to their high energy- and power-density. During each charge-discharge cycle, the ceramic undergoes transformation to a ferroelectric phase and resumes its antiferroelectric phase. The hysteresis associated with the transitions leads to a mediocre energy efficiency and service lifetime of antiferroelectric capacitors and, hence, their almost absence in commercial products. Under the support of this research project, we first formulated a universal lattice-compatibility theory that included electrostatic polarization energy along with elastic energy and thermal energy to understand the origin of the hysteresis in antiferroelectric oxides. Guided by this compatibility theory, we conducted high-throughput density functional theory (DFT) calculations to assess chemical modifiers and their effect on crystal structures of 400+ $PbZrO_3$-based compositions. Down-selected compositions were experimentally validated for their suppressed hysteresis and higher energy efficiency. The verified low-hysteresis compositions were then expanded to an antiferroelectric ceramic library with nearly 500 new compositions (more than 1,500 samples) using high-throughput experiments involving ceramic synthesis and property screening. The large quantity of data generated (theory and experimental) in these tasks were processed by machine-learning techniques and identified trends were fed to the next iteration. In the end, we successfully discovered four compositions with near-zero hysteresis, yielding a world-record energy efficiency of 98.2% at an energy density of 3.0 $J/cm^3$. Furthermore, our antiferroelectric ceramic capacitor reaches 79.5 million charge-discharge cycles lifetime, a factor of 80 enhancement over previous antiferroelectric ceramics with large hysteresis. These research accomplishments have not only met the milestones set in the SOPO, but also led to two patent filings, three journal publications (one of them was in *Advanced Materials*, impact factor 29.4), and nine oral presentations at various venues. Through the course of the project, three postdocs, four Ph.D. students, and one M.S. student were trained. In short, our project established a new methodology in searching next-generation functional ceramics on the fundamental side and discovered several high-efficiency antiferroelectric compositions for capacitors on the applied side. Once fabricated into the multilayer form for commercial applications, these ceramic capacitors can potentially enable the high temperature high power density DC-link capacitors that are critical for the next generation inverters in electric vehicles. The project also significantly contributed to the nation's workforce development in the STEM fields.

**Acknowledgements.** This technical report is based upon work supported by the U.S. Department of Energy's Office of Energy Efficiency and Renewable Energy (EERE) under the Advanced Materials and Manufacturing Technologies Office (AMMTO) Award Number DE-EE0009105.

## 1. Background and Overview

Ceramics were used as the dielectric insulators sandwiched between metallic plates of the first capacitors invented nearly a century ago. In the past decade, antiferroelectric (AFE) ceramics have shown promise as dielectrics with very high energy density while maintaining an extremely fast charge-discharge rate even at elevated temperatures. Hence, AFE ceramics could potentially be used in electric energy-storage devices for high-frequency applications of interest to EERE. Despite all their promising characteristics, AFE ceramics have not been commercially adopted due to their mediocre energy efficiency (< 80% of the stored energy can be discharged), and poor cyclability (< $1\times10^6$ cycles before short-circuiting or fracturing). This project was designed to eliminate these drawbacks by eliminating their root cause—the electric-field-induced phase transition hysteresis. The physical origin of the electric hysteresis comes from the crystallographic lattice mismatches between the AFE and the induced ferroelectric (FE) crystalline regions—they lack "lattice compatibility". These mismatches cause interfacial defects and lattice distortions that are the sources of large hysteresis. The larger the hysteresis, the lower the energy efficiency, and the shorter the service lifetime.

Our approach to decrease/eliminate this AFE/FE interfacial lattice mismatch is to apply the geometric nonlinear theory of phase transition to AFE ceramics. Previously, we successfully demonstrated this theory in metallic shape-memory alloys to eliminate hysteresis at austenite/martensite interfaces, which bears similar physical principles with what is needed for the ceramic AFE/FE interfaces. Such a perfect interface may exist if the lattice parameters of the two different phases satisfy certain constraints prescribed by the theory. We then translate these constraints into experimental parameters, such as ceramic composition to validate the theory. The iterations between theory and experiments, accelerated by machine-learning (ML) techniques, lead to identification of compositions for high efficiency, long lifetime ceramic capacitors. The specific goals of the project are:

- A powerful materials-development methodology featured with DFT-guided and ML-assisted rapid materials design, validated by high-throughput experimental synthesis and screening.
- Capacitors with bulk ceramics exhibit >3.0 J/cm$^3$ energy density, 98% charge-discharge energy efficiency, and up to $10^8$ cycles charge-discharge lifetime.

## 2. Activities and Accomplishments

### Task 1 – Universal lattice compatibility theory

The free energy density of a specimen during an electric field induced antiferroelectric to ferroelectric (FE) transition at a fixed temperature can be expressed as

$$\phi\left(\epsilon\left(\vec{\mathrm{E}},\sigma\right),\vec{\mathrm{P}}\left(\vec{\mathrm{E}},\sigma\right)\right)-\vec{\mathrm{E}}\cdot\vec{\mathrm{P}}\left(\vec{\mathrm{E}},\sigma\right)\det\mathbf{U}-\sigma\cdot\epsilon\left(\vec{\mathrm{E}},\sigma\right)+\frac{1}{2}\vec{\mathrm{P}}\left(\vec{\mathrm{E}},\sigma\right)\cdot\mathbf{D}\vec{\mathrm{P}}\left(\vec{\mathrm{E}},\sigma\right) \quad (1)$$

where, $\epsilon$, $\sigma$, $\vec{\mathrm{E}}$, $\vec{\mathrm{P}}$ denote deformation strain, stress, electric field, and polarization, respectively. $\mathbf{U}$ denotes deformation stretch tensor which can be calculated once lattice parameters are mapped in the compositional space, det$\mathbf{U}$ denotes volume change of the deformation, and $\mathbf{D}$ denotes depolarization matrix that depends on the specimen's shape. The matrix $\mathbf{D}$ is constant during the phase transition if the effect of the transition strain on the polarization of the transforming phase itself is ignored. Here, the stress is caused by the incompatibility between the two phases. In

equation (1), the first term, $\phi\left(\epsilon(\vec{\mathrm{E}},\sigma),\vec{\mathrm{P}}(\vec{\mathrm{E}},\sigma)\right)$, is the free energy of the material as a function of strain and polarization. This term is sensitive to the direction of the applied electric field and polarization. The second term, $\vec{\mathrm{E}}\cdot\vec{\mathrm{P}}(\vec{\mathrm{E}},\sigma)\det\mathbf{U}$, represents the electric energy in the material caused by the applied electric field; the third term, $\sigma\cdot\epsilon(\vec{\mathrm{E}},\sigma)$, is the elastic energy in the material associated with lattice distortions; the fourth term is the depolarization energy of the specimen with an assumed uniform polarization.

The energy difference between the forward and backward transition is then expressed as

$$\Delta\phi_{foreward}-\Delta\phi_{backward}=\Delta\vec{\mathrm{E}}\cdot\left(\vec{\mathrm{P}}_{FE}\det\mathbf{U}-\vec{\mathrm{P}}_{AFE}\right)+\Delta\sigma\cdot(\epsilon_{FE}-\epsilon_{AFE}) \qquad (2)$$

where $\Delta\vec{E}$ and $\Delta\sigma$ are, respectively, changes in the electric field and stress to circuit the antiferroelectric-ferroelectric phase transition. Equation (2) indicates that the polarization-field loop hysteresis and the stress-strain loop hysteresis together contributed to the overall free-energy hysteresis. However, polarization and strain are coupled via piezoelectric and electrostrictive effects. *We easily conclude that increasing energy density will cause a decrease in efficiency.* To separate energy density and efficiency, one must suppress charge-lattice coupling – meaning that, when the applied field moves the cations and anions, they have space to move without distorting the whole lattice. Such a scenario is possible in perovskite $ABO_3$ crystal with the Goldschmidt's tolerance factor (***t***) deviating from unity. So, tolerance factor can then be a screening factor.

**Task 2 – Density-functional theory prediction**

We employed the generalized gradient approximation (GGA)[1] for the exchange and correlation function and used the projector augmented wave (PAW)[2] method, as implemented in the Vienna Ab-initio Simulation Package (VASP)[3]. To design compositions, random distribution of substituted elements was done using supercell program[4] by taking a $2\times2\times2$ and $4\times4\times4$ supercell (320 atoms) of antiferroelectric (AFE) orthorhombic (*Pbam*) and ferroelectric (FE) rhombohedral (*R3m*) structures of $PbZrO_3$, respectively. A Γ-centered grid of $1\times1\times1$ k-point was used for geometry optimization and $2\times1\times2$ ($2\times2\times2$) k-points for the AFE (FE) phase were used for self-consistent calculations. Compositions were fully (volume and atomic positions) optimized. The convergence criterion for the relaxation and self-consistent calculations is set to $10^{-6}$ and $10^{-7}$ eV, respectively. An energy cut-off of 460 eV for plane-wave basis was used for wave functions.

Based on the results in previous literature,[5] the $(Pb,Sr,Ba,La)(Zr,Sn,Ti)O_3$ solid solution was used as the model system. **Figure 1a** shows the composition space of the B-site elements (Zr, Sn, Ti) in our investigation on the $ABO_3$ perovskite oxide. In addition, we included Sr, Ba, and La substitution on the A-site in our theoretical calculations. We focused on calculating the lattice parameters for $(Pb,Sr,Ba,La)(Zr,Sn,Ti)O_3$ compositions by optimizing their structures in the AFE and FE phases, where we monitor the AFE/FE mismatch strain, which must approach zero for a compatible interface.

We performed calculations on 400+ compositions in the solid-solution system by simultaneously varying contents of Sr, Ba, Sn, and Ti (part of these compositions are displayed in **Fig. 1b**). In addition to AFE/FE mismatch strain, we also mapped out the distortion angle of the FE rhombohedral phase primitive cell and the energy difference between the AFE and FE phases. As a rapid measure, we validated that the FE-cell angle correlates well with experimentally determined $P_{max}$ (deviations from 90° correlate to a larger $P_{max}$). The DFT energy difference between AFE and FE phases indicates the relative AFE phase stability, hence, reflects the critical

field $E_F$ of the composition. A larger absolute value of the calculated AFE stability indicates that the AFE phase is more stable, and a higher field is needed to trigger the AFE to FE transition. The FE-cell angle and AFE stability are critical factors dictating the energy density of the ceramic.

The DFT-predicted "best" 10 compositions were all experimentally fabricated and tested. The experimental results on hysteresis ($\Delta E$) and $\eta$ are plotted against the theoretically calculated AFE/FE mismatch strain in **Fig. 1c**. The correlation between AFE/FE strain and $\Delta E$ is reaffirmed, and all 10 compositions tested exhibited $\eta \geq 93.0\%$. Compositions 1 through 5 display $\Delta E < 1$ kV/cm, $\eta > 96\%$, and $W_{rec} \geq 3.0$ J/cm$^3$. Two of these compositions (#3 and #4) have an efficiency of 97.4% and 97.6%, respectively. The experimental validations shown in **Fig. 1c** demonstrate that geometric nonlinear theory is successful in guiding discovery of AFE ceramic compositions for energy-efficient capacitors.

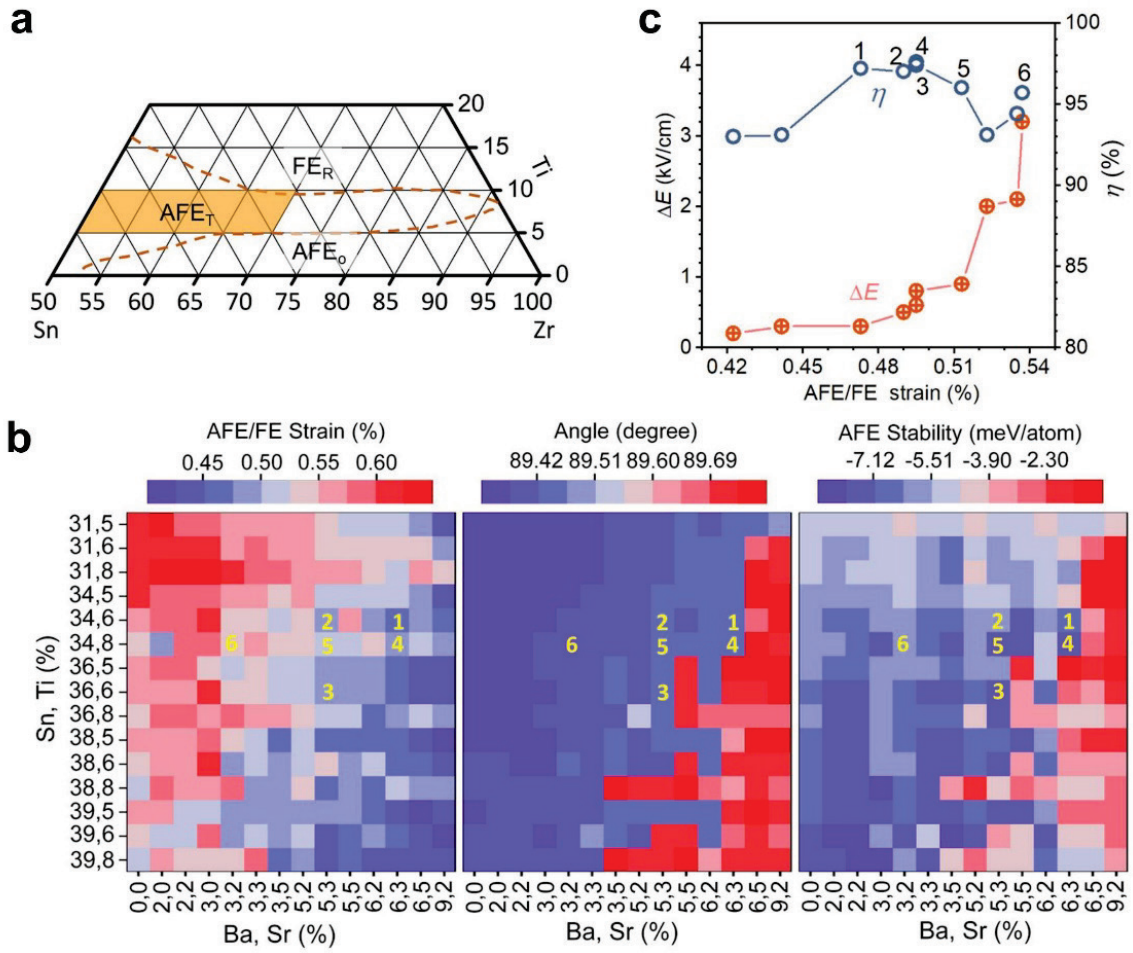


**Fig. 1.** Theory predictions of energy-efficient AFE ceramics and their experimental validations. **a**. Composition space explored is highlighted by orange shading in the ternary phase diagram. **b**. Color heat maps (from left to right) display the calculated AFE/FE mismatch strain, FE-cell distortion angle (≠90°), and the AFE stability, respectively, in compositions with varying contents of Ba/Sr on A-sites and Sn/Ti on B-sites. **c**. Experimental validations of theory down-selected 10 compositions for their $\Delta E$ and $\eta$ with respect to the calculated AFE/FE strains.

### Task 3 – Machine learning models

We demonstrated that by leveraging both DFT simulation data and data gathered from high-throughput experiments, machine learning (ML) models can be trained to probe novel regions in the composition space, and use the discovered compositions to further guide theory and experiments. We developed several families of ML models that could make actionable predictions for several different series of (Pb,Sr,Ba,La)(Zr,Sn,Ti)$O_3$ compositions. Specifically, we trained variational autoencoder (VAE) models that not only perform property prediction, but also uncertainty quantification. These uncertainty estimates served as "compositional fingerprints", and regions in the composition space corresponding to higher uncertainties indicate that more samples need to be acquired to obtain a more accurate view of the property landscape. A striking finding was that our VAE models trained on experimental data achieved very similar trends for polarization prediction as those achieved by DFT calculations (see **Fig. 2**). This gave us further evidence that our holistic integration of theory, experiments, and machine learning to enable exploring the search space for novel high-performing compositions was successful and could be used to guide experimental design in future applications.

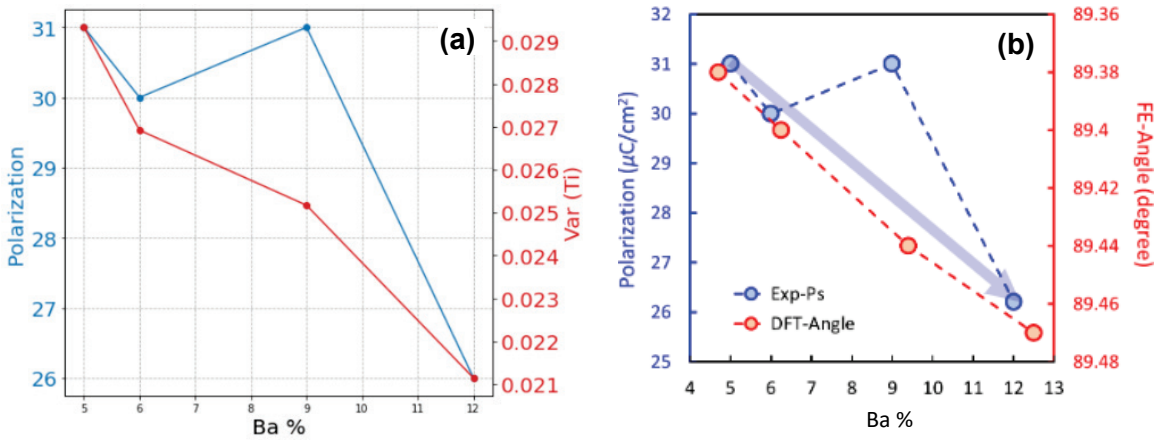


**Fig. 2.** (a) The variational autoencoder (VAE) model trained with experimental data from Task 4 reveals the trend of polarization and variance of Ti content. (b) The trend of measured polarization and calculated FE-cell distortion angle. The VAE model mirrors the DFT predictions with very similar trends.

### Task 4 – High-throughput experiments

The DFT results and ML-identified trends indicate that the (Pb,Sr,Ba,La)(Zr,Sn,Ti)$O_3$ solid solution system is promising for reaching a near-perfect energy efficiency. We used these predicted and validated compositions as starting points and broadened our composition spread by implementing a high-throughput synthesis approach to generate a library of 500+ compositions. As schematically illustrated in **Fig. 3**, this multiple-step approach involved a six-channel auto powder dispenser (batches 36 compositions in parallel), a 32-channel vibratory mill, and high-temperature box furnaces. During calcination and sintering, an arrangement of 18 crucibles (2-layer 3×3) was used to process 18 compositions in one run. Property screening was based on the polarization vs. electric field curves under unipolar fields where $\eta$ and $W_{rec}$ were quantified.

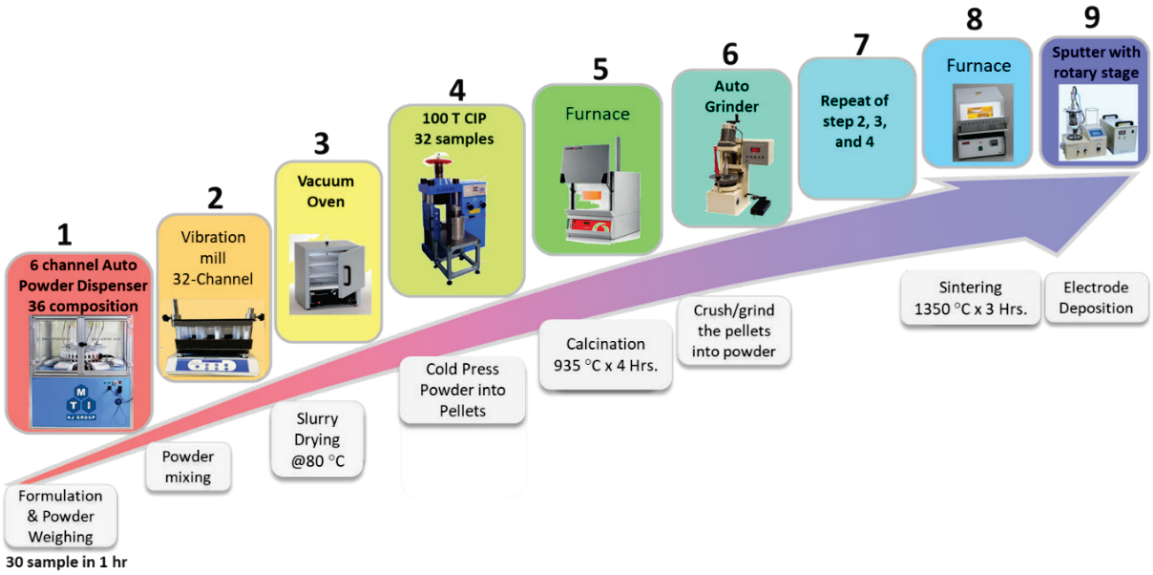


**Fig. 3**. High-throughput materials synthesis flow chart. The experimental setup is capable of fabricating 50 ceramic compositions per week.

Results of $\eta$ and $W_{rec}$ experimental measurements are illustrated in the form of heat maps, shown in **Fig. 4**. Overall, the heat map of $\eta$ is in agreement with that of AFE/FE mismatch strain in **Fig. 1b**; the heat map of $W_{rec}$ is in agreement those of FE-cell angle and AFE stability in **Fig. 1b**. Specifically, we found that Sn is beneficial to reducing $\Delta E$ and enhancing $\eta$. Increase in Ti content leads to a lower breakdown strength and a lower $E_F$ (hence, a lower $W_{rec}$); also a slight decrease in $\eta$. Substitution of Pb with Sr and Ba considerably reduces $\Delta E$ and improves $\eta$. However, their contents beyond 5 at.% lead to drop in $W_{rec}$ due to reduction in $P_{max}$ and drop in $\eta$ owing to rise in $P_r$.

Our accelerated materials synthesis and screening of 500+ compositions (3 repeats per composition) successfully identified $(Pb_{0.87}Sr_{0.05}Ba_{0.05}La_{0.02})(Zr_{0.52}Sn_{0.40}Ti_{0.08})O_3$, the best AFE composition with $\eta$ of 98.2% and $W_{rec}$ of 3.0 J/cm$^3$ (at unipolar field 220kV/cm). Near this composition, another 3 compositions are also discovered to have an energy efficiency ($\eta$) of 96.8%, 97.7%, and 98.3%, respectively, with the recoverable energy density ($W_{rec}$) around 3.0 J/cm$^3$. The two best performing compositions with $\eta > 98.0\%$ are marked by yellow stars in the left panel of **Fig. 4**. It should be noted that the energy efficiency we achieved in $PbZrO_3$-based AFE ceramics (98.2% and 98.3%) not only meets the major milestone of the project, but also makes a new world-record. These results were filed into a patent application and reported in a technical journal (*Advanced Materials*).

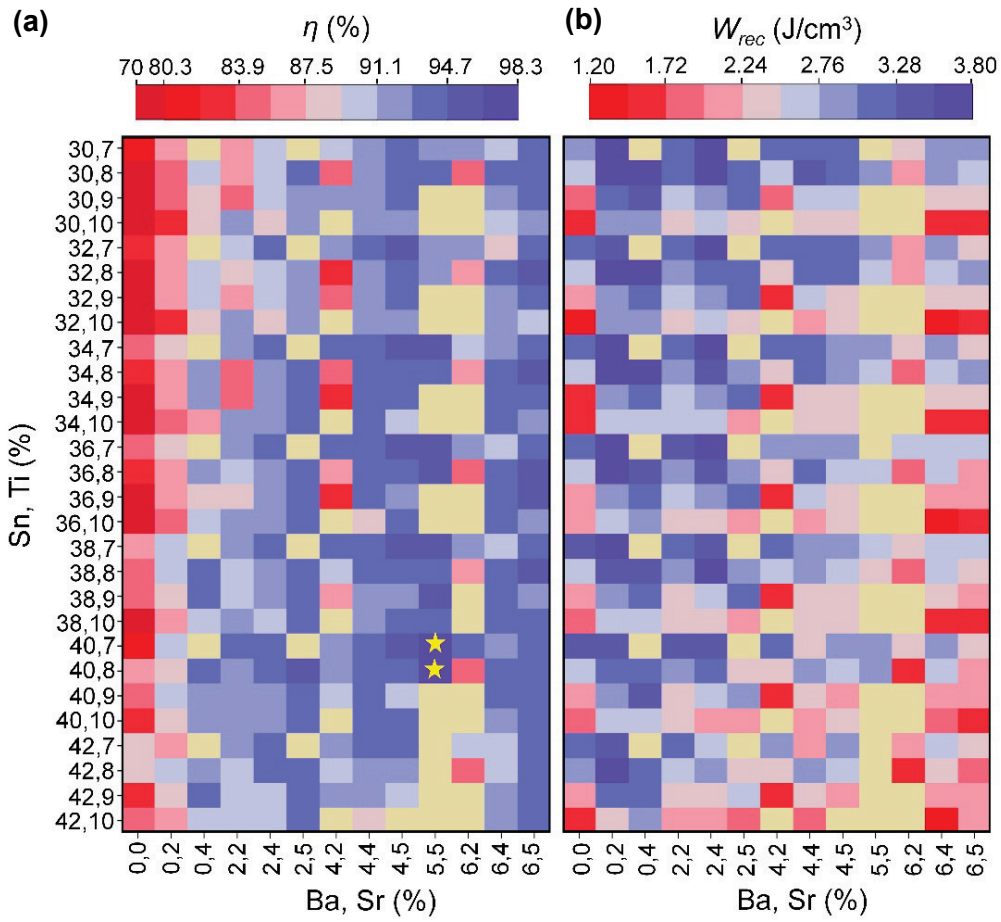


**Fig. 4.** High-throughput synthesis and property screening of $(Pb,Sr,Ba,La)(Zr,Sn,Ti)O_3$ ceramics near those discovered by theory. **(a)** The heat map of experimentally measured $\eta$. The discovered compositions with $\eta > 98.0\%$ are marked by the yellow stars. **(b)** The heat map of experimentally measured $W_{rec}$. The boxes shaded in yellow represent the compositions that exhibited very poor breakdown strength.

### Task 5 – Bulk samples and AFE capacitors

The main focus of this task was to fine tune the discovered compositions, optimize their processing conditions, and characterize in detail their crystal structures and functional properties. The $(Pb,Sr,Ba,La)(Zr,Sn,Ti)O_3$ ceramics with near-perfect efficiency require a sintering temperature of 1350°C. Such a high temperature consumes more energy and increases the production cost. Furthermore, it puts stringent requirement on the selection of electrode materials. We investigated a number of different sintering aids and discovered that $(Li_{1/2}/Bi_{1/2})$ substitution of Pb in $(Pb,Sr,Ba,La)(Zr,Sn,Ti)O_3$ ceramics is extremely effective. As shown in **Fig. 5**, we demonstrated this in the $[Pb_{0.93-x}La_{0.02}(Li_{1/2}Bi_{1/2})_xSr_{0.04}][Zr_{0.57}Sn_{0.34}Ti_{0.09}]O_3$ ceramics ($x = 0$, 0.04, 0.08, 0.12, 0.16). We found that $(Li_{1/2}/Bi_{1/2})$ substitution can significantly reduce the sintering temperature, enhance the dielectric breakdown strength, reduce the electric hysteresis, and boost the energy-storage density and efficiency. Specifically in the composition of $x = 0.12$, an ultrahigh

energy efficiency (94.0%) and a large energy density (3.22 J/cm$^3$) are achieved at a low sintering temperature (1075°C). In the late stage of the project, we demonstrated these multiple benefits of ($Li_{1/2}$/$Bi_{1/2}$) substitution in $(Pb_{0.87}Sr_{0.05}Ba_{0.05}La_{0.02})(Zr_{0.52}Sn_{0.40}Ti_{0.08})O_3$, the best AFE composition we discovered. In this composition, the sintering temperature is further reduced to 1050°C, which will allow the use of copper as the electrode in future multilayer capacitor production.

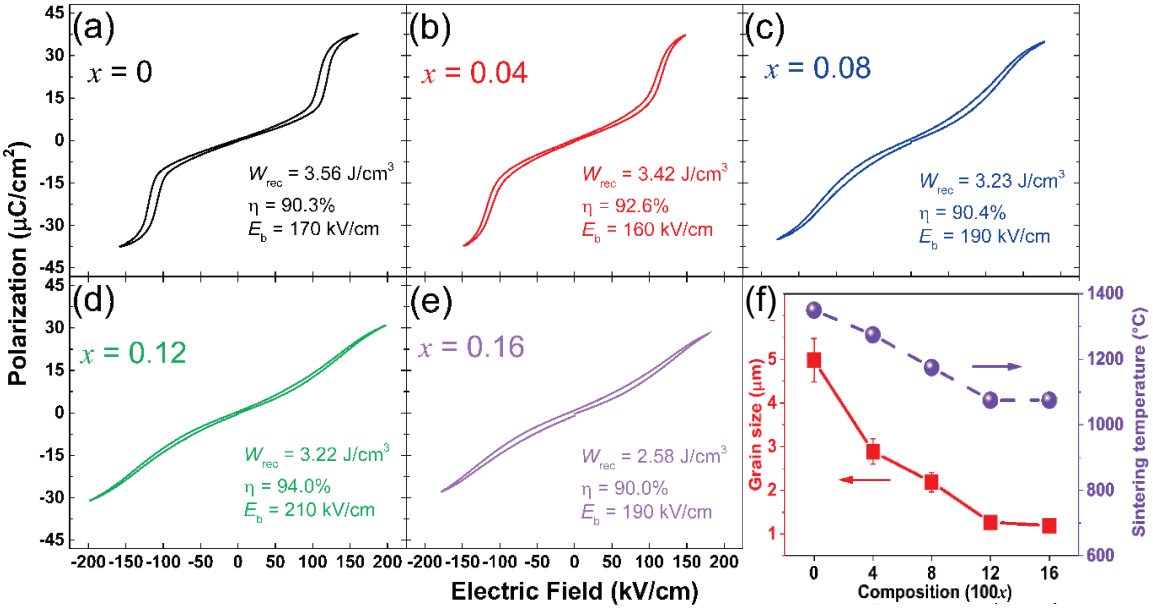


**Fig. 5.** Polarization *vs.* electric field loops of the $[Pb_{0.93-x}La_{0.02}(Li_{1/2}Bi_{1/2})_xSr_{0.04}][Zr_{0.57}Sn_{0.34}Ti_{0.09}]O_3$ ceramics measured at 1 Hz at room temperature. (a) $x = 0$, (b) $x = 0.04$, (c) $x = 0.08$, (d) $x = 0.12$, (e) $x = 0.16$. (f) Sintering temperatures and the resulting grain size in the ceramic series.

After the composition $(Pb_{0.87}Sr_{0.05}Ba_{0.05}La_{0.02})(Zr_{0.52}Sn_{0.40}Ti_{0.08})O_3$, the best with $\eta$ of 98.2% and $W_{rec}$ of 3.0 J/cm$^3$, was discovered in Task 4, we characterized the structure and properties of this ceramic in Task 5. The room-temperature structure appears to be a single-phase perovskite with tetragonal distortion. When cooled to low temperature (60 K), the ceramic adopts a monoclinic crystal structure (space group *Pm*) based on the full profile X-ray refinement. The ceramic exists as a mixture of monoclinic and tetragonal phases over the range of 180 - 220 K.

Additional measurements on electrical properties were conducted and displayed in **Fig. 6**. The dielectric constant vs. temperature curve exhibits a broad hump around 180 K, peaks at 411 K, exhibits another hump at 478 K. The dielectric constant curves measured upon heating and cooling overlap each other, revealing a near-zero thermal hysteresis for the FE–AFE phase transition (**Fig. 6a**), even though it is a first-order transition. This observation is in sharp contrast to previous $PbZrO_3$-based AFE ceramics, where a huge thermal hysteresis of 51 K was observed.[6] The result suggests that minimized AFE/FE interfacial mismatch strain enhances the reversibility of the AFE–FE phase transition triggered by both electric field and temperature. The low-temperature monoclinic phase exhibits an apparent frequency dependence of the dielectric constant (**Fig. 6b**). At 98K, the ceramic displays a single slim *P* vs. *E* loop (**Fig. 6c**). Upon increase in temperature near 170 K, the *P* vs. *E* loop begins to convert into double hysteresis loops, indicating the transition to the AFE phase. Hence, we suggest the low-temperature monoclinic phase revealed by X-ray diffraction is a FE phase. We speculate that the small electric hysteresis in the FE phase for

polarization reversal is inherited from the near-zero hysteresis in the AFE–FE transition. The polarization measurement indicates $P$ vs. $E$ double hysteresis loops remain at least up to 367 K.

Based on our hypothesis, the nearly hysteresis-free $P$ vs. $E$ curves in this ceramic is a manifestation of its compatible AFE/FE interfaces. The highly reversible AFE–FE transition engenders a strong fatigue resistance to the ceramic, surviving a record-long $7.95\times10^7$ charge-discharge cycles with only 5.8% reduction in $P_{max}$ (**Fig. 6d**). Most importantly, $\eta$ remains almost unchanged (a 1.5% loss) and $W_{rec}$ retains 91.3% of its initial value. Compared against other AFE bulk ceramics reported, our ceramics discovered by theory-guidance exhibit the highest energy efficiency and the longest endurance, particularly promising for high-frequency applications.

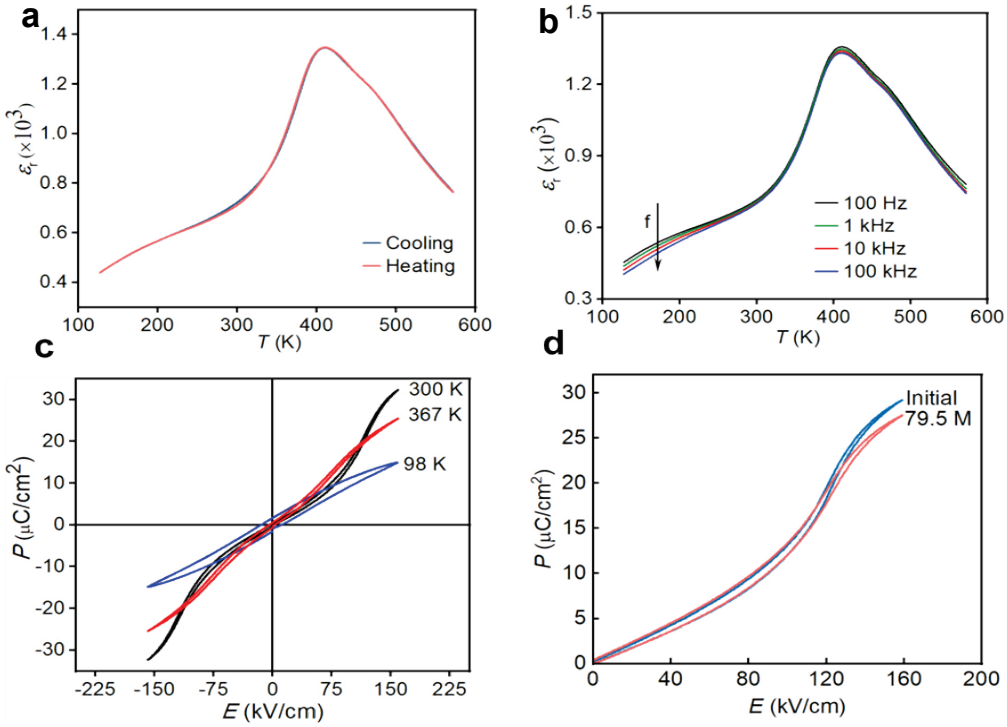


**Fig. 6.** Electrical properties of the best ceramic. **a.** Temperature-dependent dielectric constant during heating and cooling at 1 kHz. **b.** Temperature-dependent dielectric constant during heating at 0.1, 1, 10, and 100 kHz. **c.** Bipolar $P$ vs. $E$ hysteresis loops measured at 98, 300, and 367 K. **d.** Unipolar $P$ vs. $E$ curves measured at initial and after 79.5 million fatigue cycles.

## Major milestones

| Milestone | Status |
|---|---|
| **BP1.** Experimentally validate 95% energy efficiency after initial AFE oxide composition optimization. | Completed |
| **BP2.** Demonstration of an optimized AFE composition with 98% energy efficiency | Completed |
| **BP3.** Demonstration of novel AFE capacitors with energy density of >3.0 J/cm$^3$, energy efficiency of 98%, and charge-discharge lifetime of up to $10^8$ cycles | Completed |

## 3. Products and Deliverables

### Journal publications

1. P. Mohapatra, D.D. Johnson, J. Cui, and X. Tan. Effect of electric hysteresis on fatigue behavior in antiferroelectric bulk ceramics under bipolar loading. *Journal of Materials Chemistry C*, 2021, **9**, 15542-51. DOI: 10.1039/d1tc03520g. (**Journal impact factor 7.4**)

   Link: https://www.osti.gov/biblio/1827758

2. B.Z. Liu, A. Gaur, J. Cui, and X. Tan, Substitution of Pb with ($Li_{1/2}Bi_{1/2}$) in $PbZrO_3$-based antiferroelectric ceramics. *Journal of Advanced Dielectrics*, **14**, 2350022/1-8 (2024). DOI: 10.1142/S2010135X23500224. (**Journal impact factor 2.1**)

   Link: https://www.osti.gov/biblio/2319033

3. A. Gaur, R. Choudhary, B.Z. Liu, Y. Mudryk, D.D. Johnson, J. Cui, and X. Tan, Antiferroelectric ceramics for energy-efficient capacitors by theory-guided discovery. *Advanced Materials*, **36**, 2312856 (2024). DOI: 10.1002/adma.202312856. (**Journal impact factor 29.4**)

   Link: https://www.osti.gov/biblio/2370310

### Oral Presentations

1. X. Tan, D.D. Johnson, A. Gaur, B.Z. Liu, R. Renu, C. Hegde, and J. Cui. Power electronics & ceramic capacitors. An online presentation by Jun Cui to AMO project managing team on 07/14/2022.
2. B.Z. Liu, A. Gaur, R. Renu, A. Joshi, C. Hegde, D.D. Johnson, J. Cui and X. Tan. Electric hysteresis of the antiferroelectric-ferroelectric phase transition. An invited talk by X. Tan over Zoom at the 2022 Materials Science Engineering Congress, Darmstadt, Germany, on 09/29/2022.
3. X. Tan. Atomic structure, phase transitions, and functional properties of antiferroelectric perovskite oxide ceramics. An invited lecture by X. Tan at the IEEE FerroSchool Winter 2022, at University of Calgary, Canada, on 12/5/2022.
4. A. Gaur, B.Z. Liu, R. Choudhary, A. Joshi, C. Hegde, D. Johnson, J. Cui, and X. Tan. Electric hysteresis of antiferroelectric-ferroelectric phase transition. An invited talk by X. Tan at the Electronic Materials and Applications 2023 Meeting, in Orlando, Florida, USA, on 1/19/2023.
5. D.D. Johnson. Theory-guided experimental optimization of high-efficiency ceramic capacitor. An oral presentation by D.D. Johnson at the American Physical Society March Meeting, Las Vegas, Nevada. 3/7/2023.
6. X. Tan. Novel ceramic capacitors with ultrahigh energy density and efficiency. An invited panel presentation by X. Tan at the 2023 AMMTO & IEDO Joint Peer Review Meeting, in Washington D.C. on 5/18/2023.
7. B.Z. Liu. Substitution of Pb with ($Li_{1/2}Bi_{1/2}$) in $PbZrO_3$-based antiferroelectric ceramics. An oral presentation by B.Z. Liu at the 2023 IEEE International Symposium on Applications of Ferroelectrics, Cleveland, Ohio, USA, on 07/25/2023.

8. A. Gaur, R. Choudhary, B.Z. Liu, Y. Mudryk, D. Johnson, J. Cui, and X. Tan. Theory-guided discovery of antiferroelectric ceramics for energy-efficient capacitors. An oral presentation by X. Tan at the Electronic Materials and Applications 2024 Meeting, Denver, Colorado, USA, on 2/15/2024.
9. A. Gaur, B.Z. Liu, R. Choudhary, D. Johnson, J. Cui, and X. Tan. Discovery of ultrahigh efficient $PbZrO_3$-based bulk ceramic capacitors via high-throughput synthesis. An oral presentation by A. Gaur at the TMS 2024 Annual Meeting, Orlando, Florida, USA, on 3/05/2024.

**Patent applications**

1. X. Tan, B.Z. Liu, A. Gaur, J. Cui. A chemical modifier for $PbZrO_3$-based antiferroelectric ceramics to reduce fabrication temperature and improve dielectric breakdown strength. Intellectual Property Disclosure and Record filed on 10/25, 2022. Provisional patent application was filed on 5/19/2023. Patent application was filed in May, 2024. The iEdison EIR number: 3974801-22-0039.
2. X. Tan, A. Gaur, J. Cui, B.Z. Liu, D.D. Johnson, Renu. Lead zirconate-based antiferroelectric ceramics with improved energy efficiency and method of making same. Intellectual Property Disclosure and Record filed on December 14, 2022. Provisional patent application was filed on 11/27/2023. The iEdison EIR number: 3974801-22-0046.

**Website**

1. www.mse.iastate.edu/high-throughput/AFE/. This web-based database is in operation since May 2024. It allows us to share our approved data with general public. This is a download-only database without any requirement of registration. The data-approval process refers to the ISU Research Foundation Intellectual Properties review process. Typically, once provisional IP filing is complete, the team is allowed to disseminate the results to public.

## 4. Follow-up Research

Based on our two discovery disclosures, our team was invited by the Iowa State University Research Foundation to apply for the FY/2024-25 Innovation Acceleration Fund. Our application is now selected for funding to fabricate prototype devices using the best composition we discovered. Once competitive performance is demonstrated in these prototype devices, we will actively transfer our technologies to industry.

## References

[1] J. P. Perdew, K. Burke, Y. Wang, *Phys. Rev. B* **1996**, *54*, 16533.

[2] G. Kresse, D. Joubert, *Phys. Rev. B* **1999**, *59*, 1758.

[3] G. Kresse, J. Furthmüller, *Phys. Rev. B* **1996**, *54*, 11169.

[4] K. Okhotnikov, T. Charpentier, S. Cadars, *J. Cheminform.* **2016**, *8*, 17.

[5] M.J. Pan, S.E. Park, K. Markowski, W.S. Hackenberger, S. Yoshikawa, L.E. Cross, *Ferroelectrics* **1998**, *215*, 153.

[6] H. Guo, X. Tan, *Phys. Rev. B* **2015**, *91*, 144104.